BIOPHYSICS

# Distributed interfacing by nanoscale photodiodes enables single-neuron light activation and sensory enhancement in 3D spinal explants

**Agnes Thalhammer[1]*†, Mario Fontanini[1]†, Jiuyun Shi[2], Denis Scaini[1,3,4,5], Luca Recupero[1], Alexander Evtushenko[6], Ying Fu[6]‡, Suraj Pavagada[6], Andrea Bistrovic-Popov[6], Ljiljana Fruk[6], Bozhi Tian[2], Laura Ballerini[1]***



**Among emerging technologies developed to interface neuronal signaling, engineering electrodes at the nanoscale would yield more precise biodevices opening to progress in neural circuit investigations and to new therapeutic potential. Despite remarkable progress in miniature electronics for less invasive neurostimulation, most nano-enabled, optically triggered interfaces are demonstrated in cultured cells, which precludes the studies of natural neural circuits. We exploit here free-standing silicon-based nanoscale photodiodes to optically modulate single, identified neurons in mammalian spinal cord explants. With near-infrared light stimulation, we show that activating single excitatory or inhibitory neurons differently affects sensory circuits processing in the dorsal horn. We successfully functionalize nano-photodiodes to target single molecules, such as glutamate AMPA receptor subunits, thus enabling light activation of specific synaptic pathways. We conclude that nano-enabled neural interfaces can modulate selected sensory networks with low invasiveness. The use of nanoscale photodiodes can thus provide original perspective in linking neural activity to specific behavioral outcome.**

## INTRODUCTION

Next-generation approaches to understand complex neural circuits and disorders in the central nervous system (CNS) require nanotechnology-based tools to enable interfacing neuronal activity with high spatiotemporal precision and minimal invasiveness (*1*, *2*). Single-cell resolution technologies may promote modulation of cellular signals prompting new developments in bioelectronic medicine to treat CNS diseases (*3*). In addition, elucidating single-cell contribution to neural circuits and behavior may introduce transformative changes in fundamental neuroscience studies (*4*–*7*). We adopted a newly developed technology based on silicon nanowires (SiNWs), named nanoscale photodiodes (nPDs), to achieve photoelectrochemical stimulation of excitable cells (*8*). nPDs, because of their size, can be delivered in a drug-like fashion and allow light activation of cultured neurons but, differently from optogenetic approaches, in the absence of genetic manipulations (*8*). So far, the use of isolated nPDs has been reported to depolarize membranes of dissociated large neurons in culture (*8*). We asked (i) whether the mirage of minimally invasive single-cell activation could be efficiently obtained by dispersion of nPDs within a neural tissue, (ii) whether nPD length scale allows for precise targeting of individual neurons, and (iii) what are the implications of single, identified cell phenotype stimulation within network processing. Answers to these questions are crucial for developments of the future nanotechnology-based strategies in CNS interfacing (*9*). Here, we exploited wide absorption spectrum nPDs triggerable also by near-infrared (NIR) light (fig. S1), therefore suitable for applications in biological tissues (*8*). nPDs were delivered into spinal cord explants, a complex tissue where sensory-motor circuit architecture and spinal cord–resident cells are retained in a three-dimensional (3D) fashion and maintained in culture for several weeks, thus allowing the investigation of CNS development and any evolving pathology in neurologic diseases (*10*–*12*). We target the spinal cord dorsal horn (DH), a key site for somatosensory processing (*13*, *14*), to test nPDs' ability to activate individual neurons. By nPD-enabled light activation, we achieved precise excitation of a single nociceptive neuron and show that it is sufficient to potentiate dorsal network activity, potentially affecting pain signaling. Similarly, we also succeeded in activation of an individual inhibitory interneuron, which damps dorsal network activation. In such a way, we were able to show that nPDs allow dissection of the neuronal contribution to central sensory integration, providing real-time control of living cells with single-neuron spatiotemporal resolution, thus opening routes to design of minimally invasive bio-interfacing. The demonstrated ability of target stimulation to enable control in nociceptive processing might affect future strategies to treat pathological pain conditions.

## RESULTS

nPDs (Ø ~ 300 nm; Fig. 1, A and B) were synthetized as previously described (sketched in Fig. 1A and imaged in Fig. 1B) (*8*) and isolated by ultrasonication in saline solution (see Materials and Methods). In a preliminary set of experiments, nPDs dispersed at low density in saline solution were seeded onto spinal explants [organ spinal cord cultures (OSCs)]. Even distribution and deposition of nPDs on neuronal soma were shown under bright-field (BF) microscopy (Fig. 1C). We additionally quantified nPD length distribution when dispersed in cell culture medium (Fig. 1D and see Materials and Methods). We next used confocal microscopy and OSCs to selectively

[1]International School for Advanced Studies (SISSA), via Bonomea 265, 34136 Trieste, Italy. [2]Department of Chemistry, University of Chicago, Chicago, IL, USA. [3]Elettra Sincrotrone Trieste S.C.p.A., Area Science Park, I-34149 Trieste, Italy. [4]Basque Foundation for Science, Ikerbasque, Bilbao 48013, Spain. [5]Universidad del País Vasco (UPV/EHU), Barrio Sarriena s/n, 48940 Leioa, Spain. [6]Department of Chemical Engineering and Biotechnology, University of Cambridge, Cambridge, UK.
*Corresponding author. Email: ballerin@sissa.it (L.B.) athalham@sissa.it (A.T.)
†These author contributed equally to this work.
‡Present address: University of Strathclyde, Glasgow, UK.

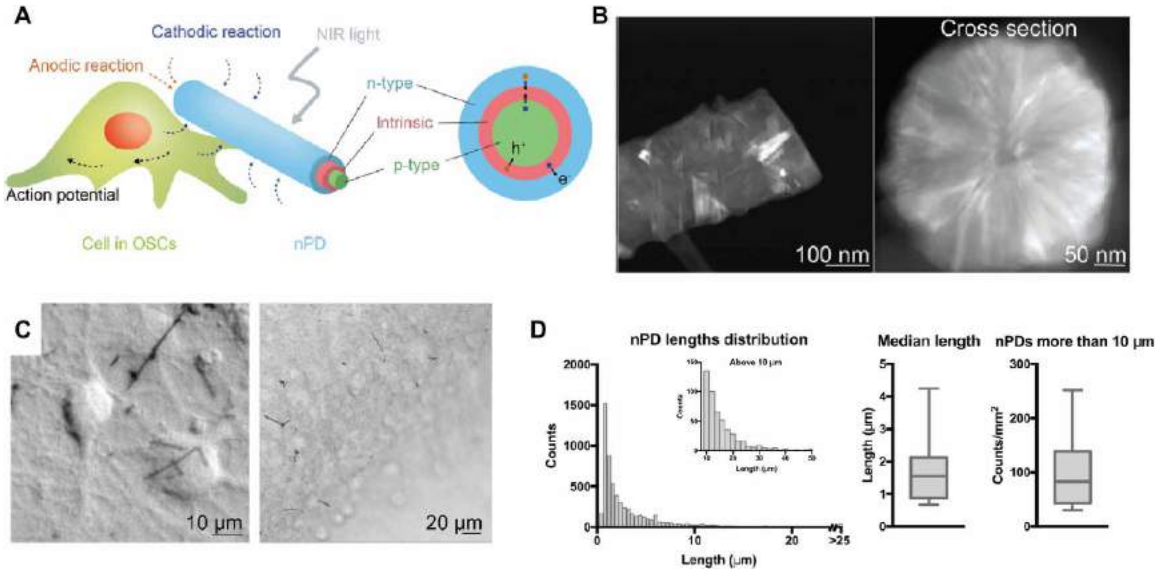


**Fig. 1. nPDs distribution in OSCs.** (**A**) Sketch of nPDs photoactivation and charges redistributed depolarizing neuronal membranes. (**B**) High-angle annular dark-field microscopy images of SiNWs with a diameter of 300 nm, side view (left) and cross-sectional view (right). (**C**) Differential interference contrast (DIC) microscopy field image of nPDs on the surface of neurons (left) and on organotypic slice cultures (right). (**D**) Length distribution of nPDs on OSC as in (C) upon washout. Note that for nPDs photostimulation, only cells in contact with 10- to 20-µm nPDs were selected. NIR, near-infrared.

photostimulate identified neurons retaining nPDs on their membrane surface (fig. S2). OSCs are ideal models for dissecting single-cell contribution to network physiology and testing because of their preserved 3D structure of sensory-motor pathways and their easy experimental access (*10*–*12*, *15*). Before live imaging experiments, OSCs were incubated for 1 to 2 hours with reconstituted nPDs (5000 pieces/µl), which spontaneously diffused within the explant slices, distributed at various tissue depths. During incubation, nPDs adhered on OSC cell body, where they were stably retained and visualized after washout (Fig. 1C and fig. S2A). We performed, in visually identified OSC neurons, live fluorescent imaging with Fluo-4 (fig. S2B), a minimally invasive approach that allows detecting neuronal activity via monitor of cytoplasmic calcium transients at a single-cell level simultaneously from a population of neurons (*16*). We stimulated nPDs (2 to 10 µm in length; Fig. 1D) by ultraviolet (UV) laser (405 nm). Figure S2 (A to C) shows the successful stimulation (125 ms, 20 mW) of the target cell displaying a large light-activated calcium transient, while neighboring neurons, without nPDs, were not activated by light.

As silicon has finite light absorption in the NIR regime (fig. S1) (*17*), a NIR (1064 nm, 20 to 25 mW) light source, which would allow for deep tissue penetration with minimal invasiveness and scattering, was used to stimulate nPDs. We validated the NIR laser illumination of nPDs success in exciting neurons (*8*) by electrophysiological recordings (see Materials and Methods). Supplementary voltage tracings in fig. S3A show nPD laser-evoked multiunit firing in OSC ventral area.

To simultaneously and selectively monitor multiple neurons, we recorded live calcium responses in cultured spinal explants by expressing the latest generation of GCaMP7f genetically encoded $Ca^{2+}$ indicators (GECIs) based on green fluorescent protein fluorescence, characterized by fast kinetics and large dynamic ranges ($k_{on}$ = 13.4 × $10^6$ $M^{-1}$ $s^{-1}$, $k_{off}$ = 5.9 $s^{-1}$, $F_{max}/F_{min}$ ≈ 30) (*18*). We further exploit the neuron-specific promotor Synapsin 1 (*19*) to restrict GECI expression to neuronal cells. Figure 2A shows low- and high-magnification OSC confocal micrographs where GCaMP7f is expressed in DH neurons visualized by neuronal nuclear protein (NeuN; Fig. 2A, left panels), a marker of postmitotic neurons (*11*). Conversely, GCaMP7f is not expressed in OSC-DH astrocytes, visualized by glial fibrillary acidic protein (GFAP; Fig. 2A, right panels), a filament protein that forms part of the cytoskeleton of mature astrocytes (*11*). Our experiments showed robust expression rates in neurons, with 48 to 95% of $NeuN^+$, but 0% of $GFAP^+$ cells exhibited GCaMP7f fluorescence, 4 to 6 days after infection (box plot in Fig. 2A; *n* = 10 fields, two cultures).

## Light stimulation of nociceptive neurons promotes long-term enhancement in spinal activity

DH neuronal hyperexcitability has long been involved in persistent pain and hyperalgesia (*20*, *21*), whose cellular and molecular mechanisms are still elusive (*22*, *23*), and we used nPDs to tackle single-neuron contribution to sensory network enhancement. Dorsal-ventral orientation of GCaMP7f-positive OSCs was identified by the presence of the ventral fissure (VF; Fig. 2B) (*10*–*12*, *15*). Typically, OSC neurons exhibited, under basal condition, a background of spontaneous neuronal activity, visualized as repetitive GCaMP7f fluorescent transients (Fig. 2D), which were completely abolished by tetrodotoxin [1 µM; a fast-inactivating voltage-gated sodium channel blocker (*24*); fig. S3B] applications. In saline solution, we delivered a localized beam (Ø15 to 20 µm) of NIR light stimulation (50 to 100 cycles of 40 ms on/40 ms off at 12.5 Hz; total duration, 4 to 8 s) targeting the selected DH cell body. We have previously reported that this frequency is most efficient for light induction of the material (*25*) as confirmed by dose response (D/R) experiments (fig. S3C and Materials and Methods). NIR activation of neurons displaying nPDs (*n* = 13 slices; see Materials and Methods) always resulted in a transient calcium response in the target cell (fig. S3D) followed in 70% of cases by DH neurons increase ($P$ = 0.016) in the frequency of calcium episodes (Fig. 2, D to F, and

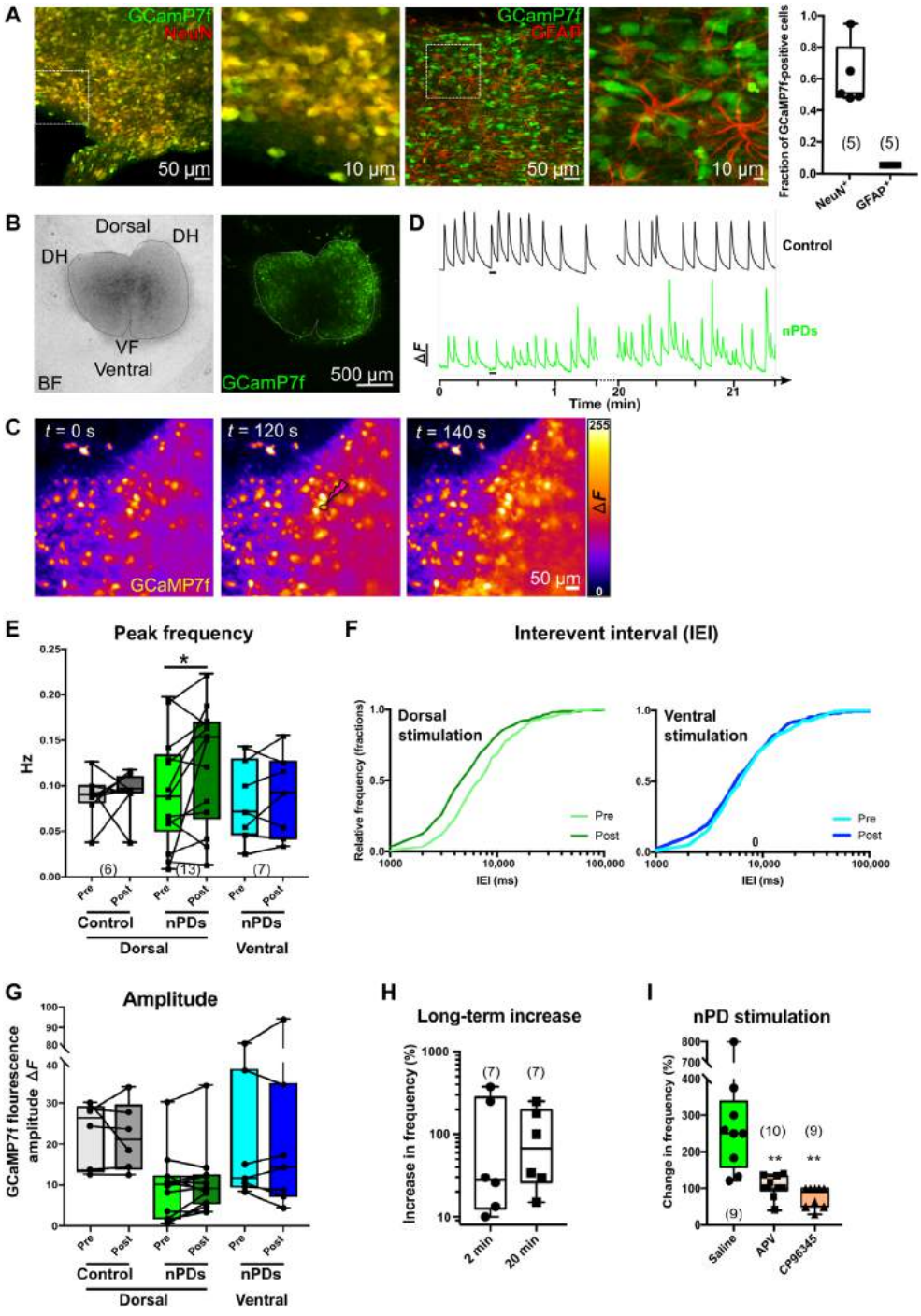


**Fig. 2. NIR light stimulation of nPDs on dorsal OSC neurons increases network activity.** (**A**) Confocal images of GCaMP7f-expressing (green) DH neurons colocalizing with NeuN (red; left) but not with GFAP (red; right). Higher magnifications from the dashed boxes. Box plot of costaining. $n = 5$ fields of view from two slices. (**B**) Low-magnification DIC image of OSC (left). DHs and VF are highlighted. Low-magnification GCaMP7f signal from the same slice (right). (**C**) GCaMP7f recording (see also movie S1) in the DH with fluorescence levels in false colors at: $t = 0$, baseline fluorescence (maximal projection of first 100 frames); $t = 120$, taken during stimulation (laser spot is highlighted with red circle); and $t = 140$, maximal projection of 100 frames after stimulation. (**D**) Mean fluorescence transient trace of ~ Ø15- to 20-µm regions of interest (ROIs) recorded before, during, and after stimulation (black bar) with NIR laser (1064 nm, 100 mW) in the absence (top; gray) and presence of nPDs (green; bottom). (**E**) Frequency of calcium events (4-min window before and after stimulation) averaged from 30 ROIs per field of view. Stimulation of a single DH neuron increased events' frequency in 9 of 13 slices (*$P = 0.016$; control, $P = 0.7551$; ventral stimulation, $P = 0.3976$; paired $t$ test). (**F**) Cumulative distribution of interevent intervals before and after nPD stimulation in DH and ventral horn (VH; $P < 0.0001$ and $P = 0.627$, respectively, Kolmogorov-Smirnov test). (**G**) Mean fluorescence amplitudes [4-min window before (pre) and after (post) stimulation] as in (E and F) ($P = 0.6425$, 0.1141, and 0.7447 for control, DH, and VH, respectively, paired $t$ test) and (**H**) box plot compare the increase (%) in frequency 2 and 20 min after nPD stimulation. (**I**) Box plot of change in frequency (%) upon nPD stimulation in saline, D,L-2-amino-5-phosphonovaleric acid (APV; 100 µM) and P96345 (100 µM). **$P < 0.01$, one-way analysis of variance (ANOVA), Tukey's post test. Numbers in brackets are number of slices.

movie S1) that was long-lasting (20 min; Fig. 2, D and H), while the amplitudes of calcium events were not enhanced upon stimulation (Fig. 2G). Similar activation of nPD neurons located in the ventral horn [VH; $n = 7$ slices; Fig. 2, E and F; $P = 0.398$ and $P = 0.627$, plots in Fig. 2 (E and F, respectively)] never resulted in post-stimulation augmentation of calcium episode frequency, suggesting that network potentiation was a specific response to repeated excitation of certain DH neurons. We never triggered cell calcium responses or network potentiation when illuminating control neurons without nPDs [control in Fig. 2 (D and E), $P = 0.7551$; $n = 6$ slices]. The lack of any fluorescent signal disturbance in the absence of nPDs also confirmed that the focused laser light did not induce any visible changes to the target neuron, the surrounding tissue, or the fluorescent dye per se.

DH neurons are a major component of circuits enabling central pain sensitization and may undergo a form of activity-dependent plasticity in response to repetitive nociceptive afferent stimulation (*14*, *21*). This results in a progressive buildup in spinal responsiveness called "wind-up" (*26*), which depends on DH activation of the glutamate *N*-methyl-D-aspartate (NMDA) receptors (*27*, *28*) possibly related to the triggering of hyperalgesia states. The light-induced long-term increase in DH activity was blocked when stimulating nPD neurons in the presence of D,L-2-amino-5-phosphonovaleric acid (100 μM, 10 min; a NMDA receptor antagonist; Fig. 2I; $n = 10$ slices; $P = 0.0043$ versus saline condition, $n = 9$ slices), suggesting the nociceptive identity of the stimulated neurons. Circuit potentiation was also blocked when nPDs were photoactivated in the presence of a neurokinin 1 (NK1) receptor antagonist (CP 96345, 100 μM, 10 min; Fig. 2I; $n = 9$ slices; $P = 0.0016$ versus saline condition), as expected since wind-up in DH is regulated through a local circuit requiring activation of NK1 receptors (*29*).

We used live labeling of TRPV1 receptors, widely present on nociceptive C-fiber presynaptic endings (*15*) and, to a minor extent, postsynaptically on DH neurons (*30*) to visually identify DH nociceptive pathways, with fluorescently (Alexa Fluor 555) tagged TRPV1 antibodies. In OSCs, we visualized the dorsal root ganglia (DRGs; see Materials and Methods) TRPV1-positive sensory neurons and fibers entering the dorsal area of the cultured slice (*31*) and positive neurons located in the DH (Fig. 3, A and B). DH neurons expressing the TRPV1 receptor have been shown to be glutamatergic (*32*). In OSC DH, TRPV1 staining colocalized with vGluT1, used to label and identify glutamatergic terminals (*33*), confirming the excitatory nature of the marked neurons ($n = 15$ fields, three slices; Fig. 3A). Upon live labeling, we singled out TRPV1$^+$ and TRPV1$^-$ neurons displaying nPDs on the cell body for selective stimulation to test whether only nociceptive neurons were involved in DH activity potentiation. Box plots in Fig. 3 (C and D) quantify these results. Light stimulation of nPD TRPV1$^+$ neurons ($n = 16$ slices) resulted in cell responses leading to a robust increase ($P = 0.0121$) in DH neurons calcium episodes; conversely, light excitation response of nPD TRPV1$^-$ cells ($n = 12$ slices), within the DH, failed to potentiate the network ($P = 0.0046$ versus TRPV1$^+$), suggesting that the network increase in activity observed after light stimulation of single DH neurons occurs via capsaicin-sensitive pathways. Thus, potentiating DH circuits requires TRPV1, NMDA, and NK1R activity, all receptors mediating central sensitization (*34*, *35*). We excluded by testing light activation of undoped SiNWs (see Materials and Methods; fig. S3E) that additional changes in local temperature, due to nanocrystalline silicon absorption of NIR light, be responsible for the selective activation of TRPV1$^+$ cells versus TRPV1$^-$ ones, confirming the pure photoelectrochemical mechanism of nPD stimulation (*8*).

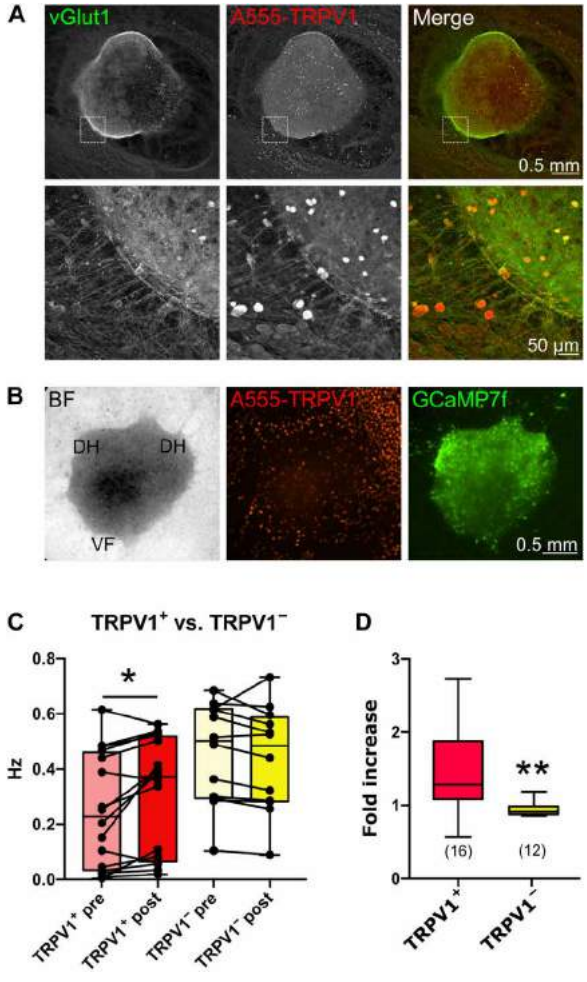


**Fig. 3. TRPV1-labeled OSC neurons and nPD light–induced increase of network activity.** (**A**) Top: Confocal images of OSCs live-labeled with Alexa Fluor 555 (A555)–TRPV1 (grayscale in middle panels and red in merge) and counterstained for excitatory marker vGlut1 (grayscale in left panels and green in merge). (**B**) Images of OSC neurons (bright field; left) live-labeled with A555-TRPV1 (middle; red in merge) and expressing GCaMP7f (green; merge in right). (**C**) Light-induced frequency increase of calcium transients in TRPV1-positive (TRPV1$^+$, $n = 16$) versus TRPV1-negative (TRPV1$^-$, $n = 12$) neurons obtained from samples as in (B). (**D**) Box plot compares the effects of nPD stimulation in TRPV1-positive versus TRPV1-negative cells, shown as fold increase (frequency after nPD stimulation normalized to the basal one before stimulation). *$P < 0.05$ and **$P < 0.01$.

## Light stimulation of nPDs on inhibitory DH interneurons depresses network activity

GABAergic interneurons make up a substantial subpopulation of DH interneurons at 2 to 3 weeks in vitro (WIV) OSC (*36*) and were identified as γ-aminobutyric acid (GABA) and NeuN double-positive cells upon fluorescence microscopy (fig. S4; $n = 15$ fields, three slices). To live label GABAergic phenotypes, we used an adeno-associated virus (AAV)–expressing tdTomato (*37*), and we confirmed their GABAergic nature by tdTomato and GAD67 (67-kDa isoform of glutamic acid decarboxylase) colocalization ($n = 15$ fields, three slices; Fig. 4A) (*38*). In a separate set of experiments, we used GCaMP7f to

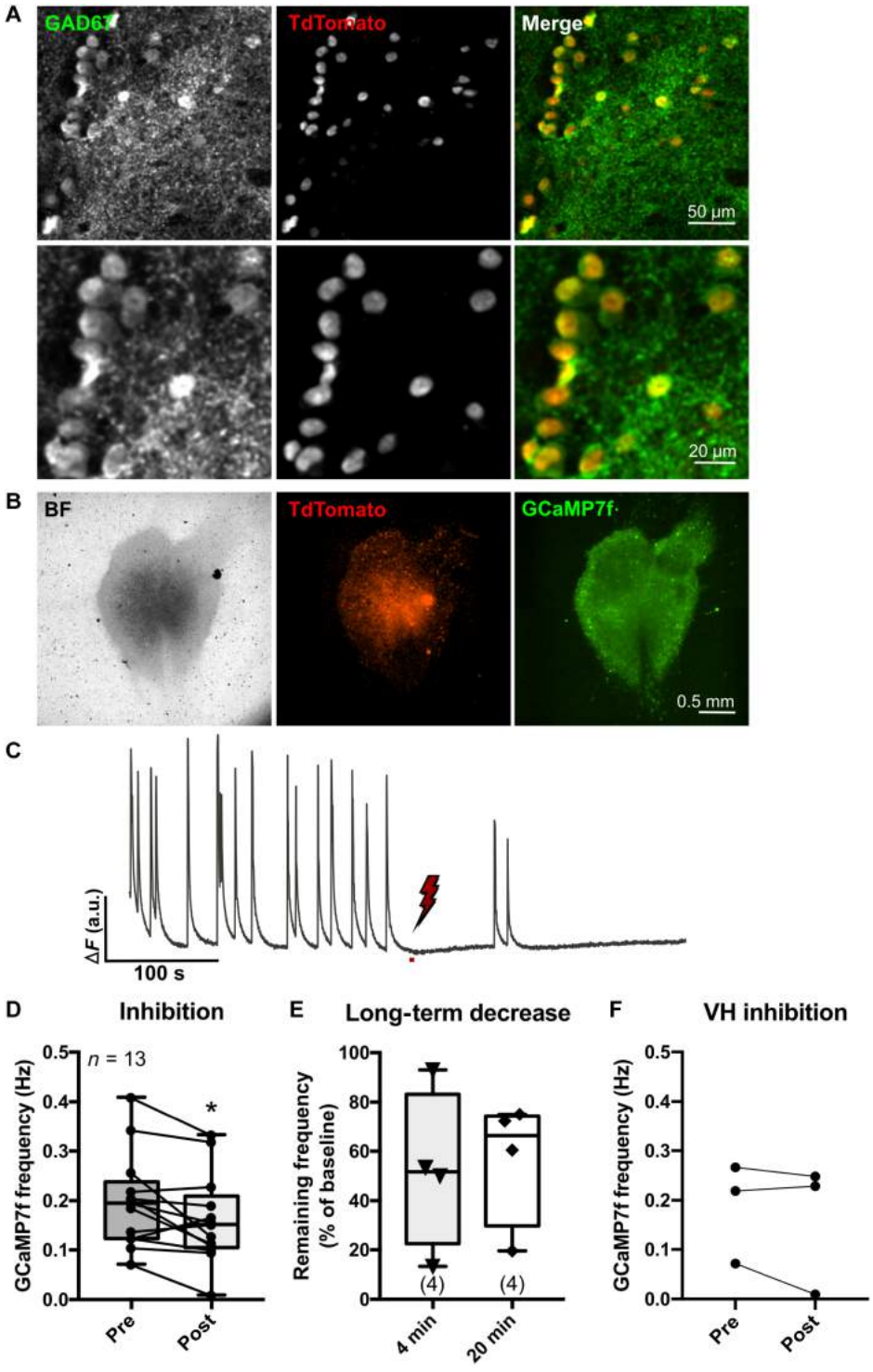


**Fig. 4. Stimulation of DH GABAergic neurons decreases network activity in OSC.** (**A**) Top: Confocal images of OSC infected with hDlx-tdTomato (grayscale in middle panel; red in merged right panel) and counterstained with GAD67 (grayscale in left panel; green in merged right panel). Bottom: Corresponding high magnification insets. (**B**) Bright-field (BF; left) image of nPD-incubated OSCs with neuronal expression of GCaMP7f (green) and GABAergic-specific expression of tdTomato (red). (**C**) Mean fluorescence transients recorded in OSCs as in (B) before and after stimulation of nPD with NIR laser. The spontaneous activity within the OSC is strongly inhibited upon stimulation of one single GABAergic interneuron. See also movie S2. a.u., arbitrary units. (**D**) Box plot quantifies experiments as in (C). *$P < 0.05$. (**E**) The suppression of network activity is long-lasting as shown by the maintenance of activity depression at 4 and 20 min after stimulation. (**F**) GCaMP7f transient frequency recorded before and after stimulation of GABAergic neurons located in the VH.

photostimulate nPDs on single tdTomato-positive neurons ($n$ = 13 slices). nPD-mediated activation (fig. S3D) of these visually identified GABAergic neurons resulted in a reduction in DH neuron calcium transient frequency in all tested OSCs (Fig. 4, C and D, and movie S2) with long-lasting depressive effects on network activity (20 min; Fig. 4E). Opposite to the neuronal network potentiation, the blocking effect was not limited to DH GABAergic neuron stimulations, in a preliminary set of experiments; in two of three OSC slices, light activation of nPDs-identified GABAergic VH neurons also induced a reduction (10 to 65%) in VH activity (Fig. 4F).

### Light stimulation of nPDs on ventral interneurons increases synchronization of neuronal activity

We further analyzed the impact of light stimulations of single non-GABAergic nPD neurons located in the VH ($n$ = 7 slices) (*10*–*12*, *36*). Ventral, premotor neurons are characterized by prominent spontaneous synaptic activity (*10*–*12*, *36*), detected as repeated calcium events (Fig. 5, A and B). In the spinal cord, a relevant feature of motor control is VH ability to synchronize rhythm-generating circuits (*39*). In OSC, the basic mechanisms underlying rhythmic spinal patterns are preserved and involve excitatory neurons (*40*); we tested whether the activation of a single VH excitatory neuron is both sufficient and necessary for augmenting synchronous rhythm generation. NIR stimulation of nPD single VH neuron, although inducing a calcium response in the target cell, was not followed by an increase in VH neuron calcium event frequency (from 0.081 ± 0.016 Hz to 0.087 ± 0.017 Hz, before and after nPD stimulation) but resulted in a notable change in VH activity patterns, characterized by a significant ($P$ < 0.0001) increase in the synchronization of calcium events among pairs of VH neurons (see Materials and Methods and movie S3), as shown by the Pearson's correlation coefficients ($r$) measured before and after single-neuron light activation (Fig. 5, C and D). NIR illumination of nPD-negative neurons did not affect $r$. In rodent spinal locomotor circuits, excitatory neurons play different roles, and rhythm generation depends on heterogeneous cell populations (*39*); thus, nPDs may offer the unique opportunity to elucidate the role of identified neurons in favoring in phase activities.

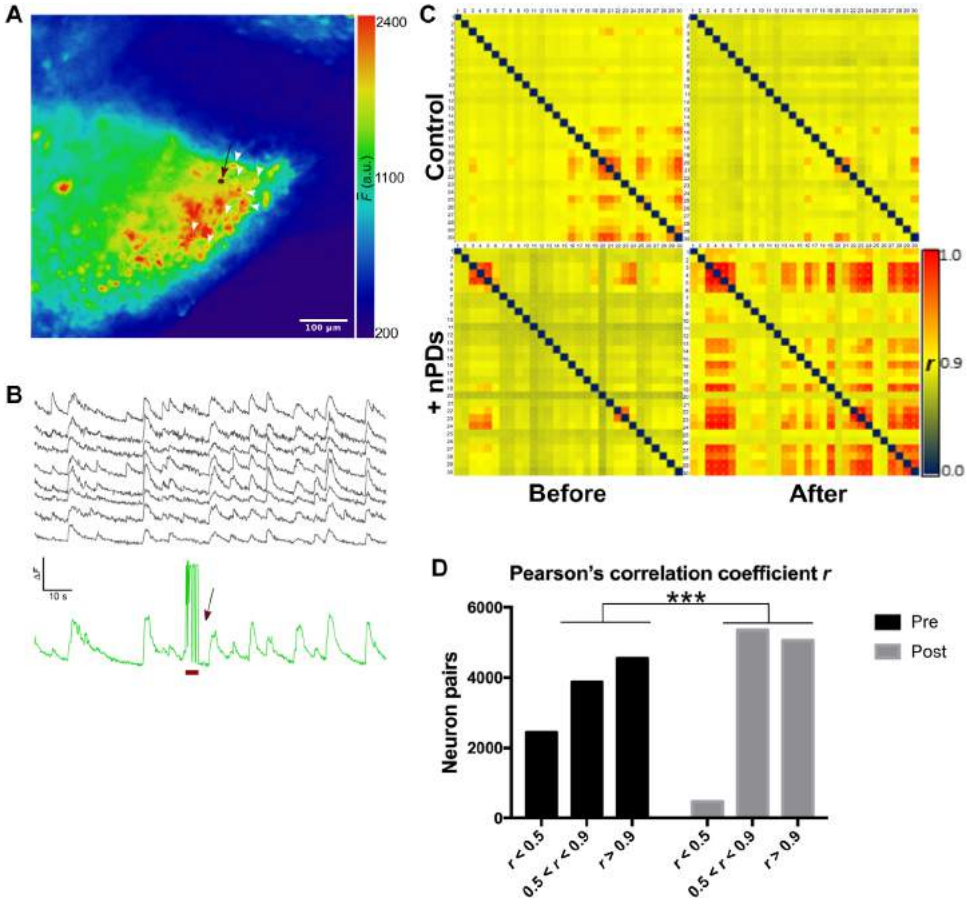


**Fig. 5. Stimulation of nPDs affects firing pattern of premotor OSC neurons.** (**A**) Low-magnification full VH field image of GCaMP7f with fluorescence levels in false colors (stimulating laser spot is visible in accompanying movie S3 from time 12:48 onward in the position highlighted with red circle and arrow in above image). (**B**) Mean fluorescence transients of representative VH ~ Ø15- to 20-µm ROIs [highlighted by yellow circles and arrowheads in (A)] recorded before, during, and after stimulation of nPDs with NIR laser (1064 nm, 80 mW). Bottom trace (in green) is taken from the stimulated neuron [red circle in (A); please note the laser artifact at stimulation]. (**C**) Heatmap representation of pairwise Pearson's correlation coefficients ($r$) of $Ca^{2+}$ transient traces from 30 neurons (numbered 1 to 30) before and after stimulation as shown in (B). (**D**) Analysis of correlation of $Ca^{2+}$ transient traces reveals significant increase in $r$ following stimulation ($n$ = 25 fields of view, ***$P$ < 0.001, chi-square test) with a shift toward higher correlation, suggesting that single-neuron stimulation sets the overall in-phase activity and coordination in the spinal cord.

### nPDs functionalized with antibodies against the GluA2 subunit of AMPA-type glutamate receptors: Direct light activation of DH excitatory pathways

We further explored the possibility of directing the nPDs to subcellular structures, such as synaptic receptors, to activate specific signaling pathways by NIR light stimulation of neurons carrying tightly anchored nPDs in virtue of their integrated membrane proteins. We chose the GluA2 subunit of AMPA-type glutamate receptors as the target molecule to hook nPD localization within the DH excitatory synapses. Antibodies against GluA2, able to live label glutamate AMPA receptors (*41*), were linked to nPDs (sketched in Fig. 6A) through maleimide functional group introduced through coupling

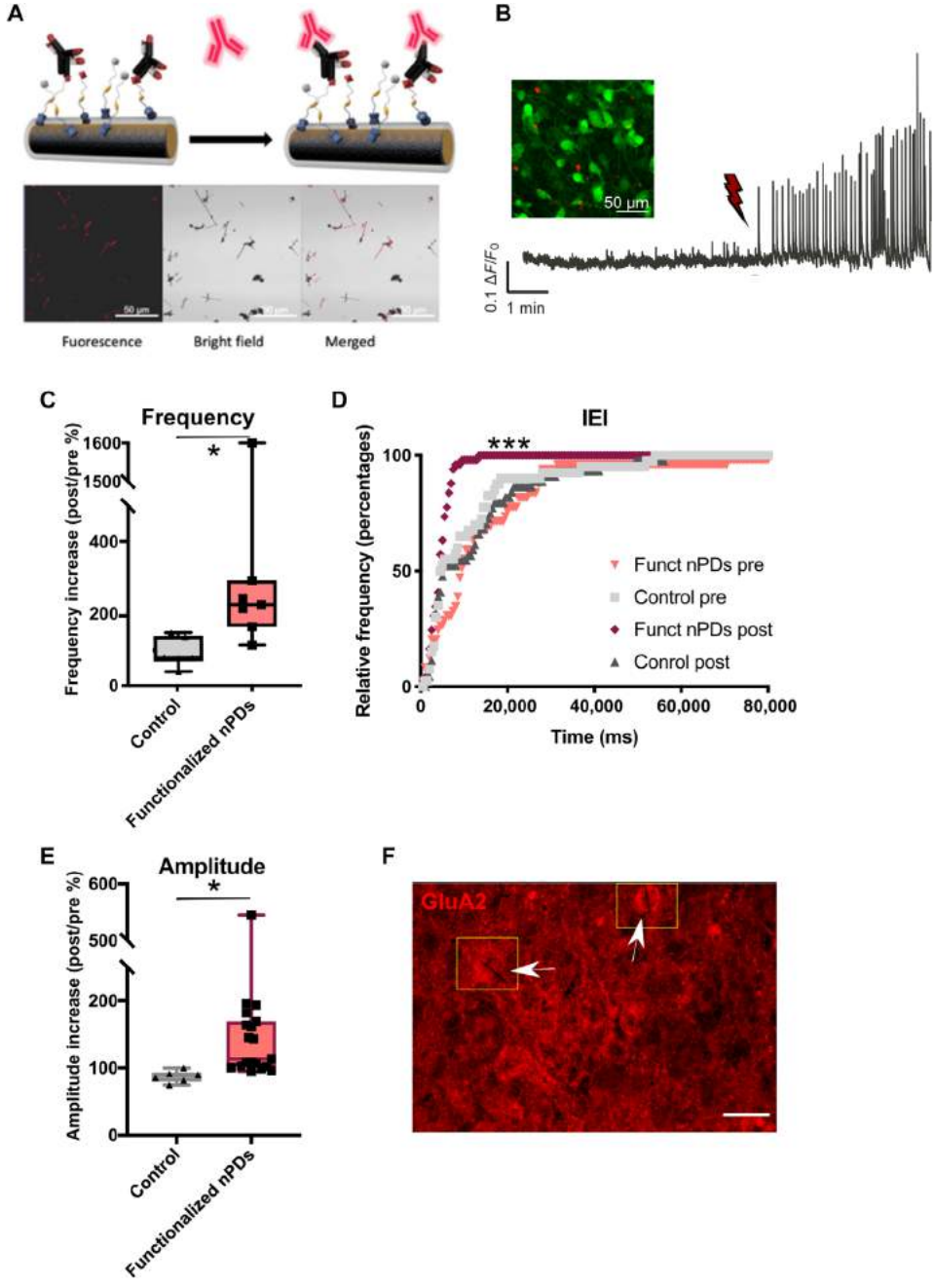


**Fig. 6. Functionalization with GluA2 antibodies directs nPDs to DH excitatory pathways.** (**A**) Top: Sketched antibody-functionalized nPDs using silane-based linker. Bottom: Visualization of immobilized antibodies via fluorescent probe-linked secondary antibodies. (**B**) Inset: Confocal image of OSCs expressing neuronal GCaMP7f (green) incubated with GluA2 functionalized nPDs (in red). Example of GCaMP7f fluorescent transients reveals strong increase in network activity upon light stimulation of functionalized nPDs. (**C**) Quantification of increase (%) in frequency of calcium transients as in (B). (**D**) Cumulative distribution of interevent intervals (IEI) before and after stimulation of control (gray) and GluA2-functionalized (pink) nPDs. ***$P < 0.001$. (**E**) Quantification of increase (%) in amplitude of calcium transients as in (B). $n = 6$ slices without nPDs and $n = 8$ slices with functionalized nPDs. *$P < 0.05$, Student's $t$ test with Welch's correction. (**F**) Confocal image of GluA2-functionalized nPDs (arrows) on OSC, immunostained for GluA2. Note that nPDs appear as lack of fluorescent signal on the background of GluA2-stained cells (ROIs).

to amino-silane [(3-aminopropyl)triethoxysilane (APTES); fig. S5]. Successful nPD-antiGluA2 linkage was confirmed by electrochemical impedance spectra (see Materials and Methods) and by imaging of functionalized nPDs using fluorescently labeled antiGluA2 (Fig. 6A). Incubation of the functionalized nanomaterial with OSCs resulted mostly in nPD-antiGluA2 localization on GCaMP7f neurons in the DH [Fig. 6, B (inset) and F]. Selective NIR light stimulation of nPD-antiGluA2 ($n = 3$ slices) induced a substantial increase ($P = 0.0328$) in calcium event frequency (Fig. 6, C and D) and amplitude (Fig. 6E) throughout the neuronal network. The potentiation in frequency was in accordance with what was observed when stimulating nPDs on DH TRPV1$^+$ (excitatory) neurons. Notably, light stimulation of nPDs functionalized toward AMPA receptors also augmented calcium event amplitude. We cannot exclude that a direct hook of AMPA receptors by nPDs affected receptor biophysics upon nPD activation, such as the kinetic, calcium permeation, or voltage rectification or that AMPA receptor turnover is altered when linked to nPD-antiGluA2, all factors potentially leading to a stronger potentiation of glutamatergic postsynaptic signaling. Alternatively, the closer location of nPDs to the neuronal membrane, due to the antiGluA2 functionalization, led to a more efficient light-induced depolarization driving neuronal excitation, thus favoring the circuit facilitation. Single-molecule targeting of functionalized nPDs (Fig. 6F) allows precise distribution on glutamatergic pathways of delocalized nPD delivery and offers new research tools and potentially new therapeutic strategies.

## DISCUSSION

Our major result is the successful exploitation of nanoscale photoactivable devices with a length matching the dimension of neuronal cell body, thus enabling NIR-light noninvasive stimulation of single neurons identified within the complex sensory-motor architecture of spinal cord explants. nPDs behave as wireless neural modulator, locally tune the neuronal membrane polarization, and ignite action potentials (*8*). nPDs also activate neurons diverse from TRPV1-expressing ones [a lineage also required for thermal sensation (*42*, *43*)] such as GABAergic cells or VH excitatory ones, ruling out the possibility of mere heat activation of neurons due to SiNW photoexcitation. nPD photothermal activation was further excluded (*8*) by NIR light testing of undoped SiNWs.

The nPD reliability in selective stimulating the target cell is strengthened by the opposite and reproducible network outputs tuned by the phenotype and location of the activated neuron. nPD technology allows us to obtain on an epifluorescence microscope the exclusive light activation of the identified cell, with high single-neuron spatial resolution (see Materials and Methods and fig. S2D) and potentially avoiding the so-called cone influence (*44*) that, in optogenetic strategies coupled to photoactivation, influences a volume of the illuminated tissue, which usually includes neighboring neurons. nPDs represent a real single-cell perturbative system without coexcited cells, a novel promising tool to probe sparse network coding or single-cell contribution to network behavior and processing in fundamental neuroscience.

Local DH elaboration of sensory information comprises a complex network of excitatory and inhibitory interneurons, and dysfunctions within DH circuitry are known to be involved in pathological pain conditions (*45*). Recent advances in spinal cord optogenetics combined to fluorescence imaging techniques have been used to investigate peripheral and central sensory processing (*46*). By nPD interfacing, we show that activating even a single nociceptive CNS neuron could sustain enhanced excitatory signaling; likewise, a single inhibitory interneuron might inhibit network activity. This approach could provide the opportunity to define somatosensory circuitry and to design therapeutic approaches with unprecedented detail. In addition, the use of NIR light to excite nPDs offers novel opportunities in neuronal photoactivation when embedded in 3D tissues, mitigating scattering of light (greater with short wavelengths) and allowing light to penetrate deeper into the tissue.

A further step in nPD nanotechnology is provided by their functionalization to target a single molecule and, in our experiments, expanding the potential of nanoscale photoactivable devices to be localized at precise subcellular site, allowing stimulation of glutamatergic signaling pathways with single-cell precision. Besides fundamental studies, our results might have implications for future clinical therapeutics in intact spinal cord. Although, in the current work, nPDs are tested in immature tissue cultures, their functional stability, the absence of cell internalization, and the absence of resident cell reactivity upon 24 hours exposure in OSC (see Materials and Methods and fig. S6) are all indicators of nPDs' biomedical potential. As with the optogenetic strategies (*47*), there are substantial challenges still to overcome to enable real-world translational application of this technology in the spinal cord. However, we believe that nPDs will be relevant when localized and less invasive interfacing is desirable to treat dysfunctional signaling in the CNS. Our study is the first step toward real-life biomedical application.

## MATERIALS AND METHODS

### Animal care

All experiments were performed in accordance with the European Union (EU) guidelines (2010/63/UE) and Italian law (Decree 26/14) and were approved by the local authority veterinary service and by our institution (SISSA) animal well-being committee (OBPA). All efforts were made to minimize animal suffering and to reduce the number of animals used. Animal use was approved by the Italian Ministry of Health (no. 22DABN1WO and 22DABNYQA), in agreement with the EU Recommendation 2007/526/CE.

### Preparation of nPDs

nPDs were synthesized through the chemical vapor deposition process as previously reported (*8*). nPDs have a coaxial layered structure with p-type silicon core, intrinsic silicon shell, and n-type silicon outer shell. During the chemical deposition process, silane ($SiH_4$), diboron [$B_2H_6$; 100 parts per million (ppm) in $H_2$], phosphine ($PH_3$; 1000 ppm in $H_2$), and hydrogen ($H_2$) were used as the silicon precursor, p-type dopant, n-type dopant, and carrier gas, respectively. In a typical experiment, Si <100> wafers (0.001 to 0.005 ohm·cm; n-type, Nova Electronic Materials) were first decorated with citrate-stabilized gold colloidal nanoparticles (diameter, 50 nm; Ted Pella) on the surface as the catalysts. The p-type core was grown at 470°C at a pressure of 40 torr with the silane flow rate of 2 standard cubic centimeters per minute (sccm), diboron (100 ppm in $H_2$) flow rates of 10 sccm, and hydrogen flow rate of 60 sccm for 30 min. Then, the synthesis process was paused in vacuum for 20 min. Then, the intrinsic silicon shell was grown at 750°C at a pressure of 20 torr for 15 min with the silane and hydrogen flow rate of 0.3 and 60 sccm, respectively. The n-type outer shell was grown at the same temperature

and pressure condition as the intrinsic layer with the additional phosphine at the flow rate of 1.5 sccm for 15 min.

### Preparation of undoped SiNW

The undoped SiNW was synthesized by chemical vapor deposition. In a typical procedure, silane ($SiH_4$) and hydrogen ($H_2$) were used as the silicon precursor and the carrier gas, respectively. The intrinsic core was grown at 480°C at a pressure of 40 torr with the silane flow rate of 2 sccm, and hydrogen flow rate of 60 sccm for 30 min. Afterward, the synthesis process was halted in vacuum for 20 min. Last, the intrinsic silicon shell was grown at 750°C for 30 min at a pressure of 20 torr with a silane and hydrogen flow rate of 0.3 and 60 sccm, respectively.

### nPDs reconstitution

The wafer containing nPDs was cut into 1 cm–by–1 cm pieces, tipped into 30% HF, washed three times, transferred into a 2-ml Eppendorf tube, submerged in 1 ml of isopropanol, and ultrasonicated for 30 min at 40°C. After removing the support piece from the nPD suspension with tweezers, the isopropanol was let to evaporate in oven at 80°C. nPDs were resuspended in 0.5 ml of sterile Gey's balanced salt solution (GBSS) under a flow hood and concentration optically determined.

### Preparation of organotypic cultures

OSCs of spinal cord and DRG were prepared as described previously (*10*, *11*, *36*). Briefly, pregnant mice were exposed to a $CO_2$ overdose and decapitated, and fetuses were delivered by cesarean section. Isolated fetuses were decapitated, and their backs were isolated from low thoracic and high lumbar regions and transversely sliced with a tissue chopper. Slices (275 μm) were cleaned by dissection in GBSS to obtain the spinal cord and DRGs; fixed on a glass coverslip with fibrin glue, i.e., reconstituted chicken plasma (Rockland) clotted with thrombin (Merck); and cultured in 1 ml of medium [Dulbecco's modified Eagle's medium (Life Technologies, no. 31966-021) supplemented with 25% fetal bovine serum (FBS; Life Technologies, no. 10500-064), 1× B27 supplement (Life Technologies, no. 17504044), 1× penicillin-streptomycin, and mouse nerve growth factor (10 ng/ml)] in flat-bottom 15-ml screw cap tubes under rotation in an incubator at 37°C and 5% $CO_2$. Experiments were performed after 2 to 3 weeks in vitro.

### Preparation of hippocampal cultures

Hippocampal primary cultures were prepared as previously described (*33*). Briefly, hippocampi isolated postnatal day 0 to 3 Wistar rats were digested by three separate enzymatic [trypsin (5 mg/ml; Sigma-Aldrich, no. T10051), deoxyribonuclease type I (0.75 mg/ml; Sigma-Aldrich, no. D5025-150KU), trypsin inhibitor (2.5 mg/ml; Sigma-Aldrich, no. T9003)] and mechanic steps alternated with washings [4.2 mM $NaHCO_3$, 12 mM Hepes (Merck, no. 4034), 200 μM kynurenic acid (Sigma-Aldrich, no. K3375), 25 μM D-AP5 (Abcam, no. ab120003), powder Hank's modified (Sigma-Aldrich, no. H-2387), 33 mM glucose, bovine serum albumin (BSA) fraction V (0.3 mg/ml; Merck, no. 10735086001), 12 mM $MgSO_4$, and gentamycin (0.25 μl/ml; Sigma-Aldrich, no. G12)]. The final pellet of cell was resuspended in Neurobasal medium [1× Neurobasal-A Medium (Gibco, no. 10888-022) supplemented with 1× GlutaMAX (Gibco, no. 35050-061), 1× B27 supplement (Life Technologies, no. 17504044), and gentamycin (0.5 μl/ml; Sigma-Aldrich, no. G1272)]. Cells were then plated on a 12 mm–by–24 mm coverslip (150,000 cells per coverslip) pretreated with poly-L-ornithine (Sigma-Aldrich, no. P4957) and maintained (7 to 10 days in vitro) in an incubator at 37°C and 5% $CO_2$.

### Fluo-4 live calcium imaging

nPDs reconstituted in GBSS were cocultured with OSCs for 2 hours. One hour before recordings, OSCs were incubated with 1 μM Fluo-4 AM and washed for 30 min before recording. To visualize the nPDs along with the fluorescent components, the reflection mode setting was used on a Nikon A1R confocal microscope and images were acquired at 6 frames per second (fps). Before setting the NIR light laser stimulation, we pretested the responses of OSC neurons to light stimulation when, on cells decorated by several nPDs, we focused on one nPD by confocal microscopy. Stimulation was achieved in resonance mode as setup for uncaging protocols via the UV laser [405 nm, 126 × 126 pixel region of interest (ROI) in a field acquired with a 40× oil immersion objective Plan Apo numerical aperture (NA) 0.95 at zoom 8].

### Electrophysiological recordings

Under the same experimental conditions as those described for live imaging (see below), extracellular recordings were obtained from the ventral area of the spinal cord by placing a 2 M NaCl-filled glass micropipette (4 to 5 megohm) alongside the median VF of the slice. Fast voltage transients (multiunit potentials) could be attributed to the firing of action potentials in neurons near to the recording electrode tip, including the nPD stimulated one. Signals were amplified via MultiClamp 700B Axon CNS Molecular Devices and were detected via Axon Digidata 1550B Low-Noise Data Acquisition System. The amplifier's gain was set at 100 × AC membrane potential (100 mV/mV). Multiunits associated to the firing of action potentials in neurons nearby both the pipette tip and the point of laser stimulation could be visibly distinguished from spontaneous laser-unsolicited transients.

### Virus preparation and infection

pGP-AAV-syn-jGCaMP7f-WPRE was a gift from D. Kim and GENIE Project (Addgene plasmid no. 104488; http://n2t.net/addgene:104488; RRID:Addgene_104488) (*18*) and pAAV-hDlx-GqDREADD-dTomato-Fishell-4 was a gift from G. Fishell (Addgene viral prep no. 83897-AAV1; http://n2t.net/addgene:83897; RRID:Addgene_83897) (*37*). AAV1/2 viruses were prepared as described previously (*48*). Briefly, ten dishes (15 cm) of human embryonic kidney 293T cells at 80% confluency were transfected with plasmids of capsid (pRV1), helper (pFdelta6), and cargo (pGP-AAV-syn-jGCaMP7f-WPRE with ratio 1:4:2) with PEI reagent (plasmid:PEI = 1:11; Sigma-Aldrich). Six days after transfection, cells and media were collected. The mixture was then centrifuged at 3700*g* at room temperature (RT) to remove cellular debris and further concentrated by ultrafiltration using a crossflow cassette VivaFlow 200 (Sartorius, no. VF20P4). The purified AAV particles were collected after purification of the viral concentrate via a discontinuous iodixanol gradient column (OptiPrep density gradient medium; Merck, no. D1556-250ML) in an ultracentrifuge at 44,400 rpm (type 70 Ti fixed-angle titanium rotor; Beckman, no. 337922) for 2 hours at 18°C (Beckman, L8-70M) by manual collection of the respective phase, which was further filtrated using a 100-kDa cut-off filter (Merck, no. UFC910008) in several steps, diluting with phosphate-buffered saline (PBS), to changing the buffer to PBS and concentrate the sample to about 250 μl. For infection, OSCs were incubated with virus diluted 1:2000 to 1:5000

in culture medium at days in vitro (DIV) 12 to 15. For GABA labeling, OSCs were coinfected with AAV1 virus carrying hDlx-dTomato to achieve expression of dTomato in GABAergic cells and AAV1/2 for GCaMP7f expression at a ratio of 1:1.

### Live calcium imaging with GCaMP7f and image analysis

OSCs expressing GCaMP7f in neurons were recorded in a custom 3D-printed perfusion chamber mounted on a Nikon microscope (Nikon Eclipse Ti2 microscope endowed with a Nikon Intensilight Hg lamp and an Andor Zyla sCMOS). Extracellular saline solution [152 mM NaCl, 4 mM KCl, 2 mM $CaCl_2$, 1 mM $MgCl_2$, 10 mM Hepes (Merck, no. 403), and 10 mM glucose (pH 7.4); osmolarity adjust to 300 mosM], was perfused with a flow-rate of 5 mL/min. For stimulation of nPDs, we selected cells displaying, when visualized in BF and differential interference contrast microscopy before fluorescence recordings, one SiNW on their soma and we used a Chromacity 1040 air-cooled, compact ultrafast ytterbium fiber laser emitting at NIR wavelength (1064 nm) via a High-Speed Meadowlark Spatial Light Modulator (MSP1920-1064-HSP8-C) coupled to the backside infinite path of the microscope. The laser light passed through a Thorlabs SH05/M shutter controlled by a Thorlabs KSC101 to allow temporal patterning of stimulation. The full laser beam was concentrated to a spot of Ø15 to 20 μm with a measured total laser power to the sample of 20 to 25 mW (D/R plot in fig. S3C) except for a maximum intensity of 80 mW used only for the representative experiment depicted in Fig 5. GCaMP7f fluorescence was visible with a 4× Plan Fluor NA 0.13 air objective or a 20× S Plan Fluor ELWD NA 0.45 objective with 100 and 5 ms of exposure, respectively, when using ND filter 32 for the excitation light and imaged with the latter objective at a sampling rate of 6.6 fps and 4 × 4 binning. $Ca^{2+}$ fluorescence recordings were started upon identification of a slice area that displayed the presence of nPDs on cell bodies and neuronal spontaneous activity.

The acquired time series of images recorded from the selected field (size, 636.4 μm by 636.4 μm) were analyzed in Fiji choosing 20 to 30 ROIs of ~ Ø15 to 20 μm placed onto the cell soma, and the obtained mean fluorescence traces were processed in Clampfit 10.7 (Molecular Probes). For dose-response curves, a Thorlabs ND filter wheel (0.04 to 4 in 10 steps) was inserted into the laser path and the laser power used for stimulation was increased stepwise by manually changing the position of the filter wheel. The percent increase in frequency was plotted against the laser power and fitted in Igor Pro 6 with a sigmoid fit using the equation $f(x) = a + b/(1 + e^{-(x-c/d)})$, with $a$, $b$, $c$, and $d$ being 106.74,114.83, 18.484, and 1.0776, respectively. fi = W_coef[0]+W_coef[1]/(1 + exp.(−(x − W_coef[2])/W_coef[3])) with W_coef = {106.74, 114.83, 18.484, 1.0776}.

In a different set of experiments, we used hippocampal cultures where the NIR light activation of nPDs placed at <8-μm distance from the recorded neuron (fig. S2d) did not result in changes in calcium episode frequency or amplitude of the observed cell, suggesting that direct contact between nPD and neuron was a prerequisite for effective nPD activation by the light stimulus.

### TRPV1 live labeling

Rabbit anti TRPV1 antibody (25 μg; Synaptic Systems, no. 444 003) were labeled with Alexa Fluor 555 Microscale Protein Labeling Kit (Thermo Fisher Scientific, no. A30007) according to the manufacturer's description but using the recommended 10× dye/protein ratio to ensure labeling despite the presence of BSA. OSCs were incubated with labeled antibody (25 μg/ml) for 2 hours or, alternatively, unlabeled antibody (10 μg/ml) for 90 min followed by washing three times for 15 min (recording solution) and 90-min incubation with a 1:200 dilution of Alexa Fluor 594 goat-anti-rabbit antibody (Invitrogen, no. A-11012). Antibodies were all incubated in medium at 37°C under rotation, and nPDs were added 1 hour before the end of the incubation. Once nPDs had been added, the slices were kept in the incubator without agitation to favor nPD penetration in the tissue.

### Functionalization of nPDs

Chips (1 cm by 1.8 cm) cut from the nPD wafer were surface-treated using a Femto Plasma Cleaner (Diener Electronic) for 5 min. Each chip was immediately submerged in 10.9 ml of methanol, 0.58 ml of Milli-Q water, 0.12 ml of APTES (Sigma-Aldrich), and 0.55 μl of acetic acid and left under agitation overnight. Chips were removed from solution, washed with isopropanol and water three times, dried under nitrogen, and incubated at 90°C for 1 hour. Following the wash and drying steps, each chip was again submerged but, this time, in the solution of 2.2 ml of dichloromethane and 8.2 μl of triethylamine containing 11 mg of 4-maleimidobutyryl chloride. After overnight agitation, they were washed with isopropanol and water three times, dried under nitrogen, and incubated with 3.5 ml of 1× PBS containing 25 μg of GluR2 monoclonal antibody (6C4) (Invitrogen, no. 32-0300) overnight. The antibodies were prepared by adding 50 μl of antibody solution (500 μg/ml) to 450 μl of P/E/MES buffer (5 mM EDTA; Thermo Fisher Scientific) and 10% MES (Fisher Bioreagents) in 1× PBS containing 0.2 μg of tris(2-carboxyethyl)phosphine (Thermo Fisher Scientific), incubating under agitation for 1 hour and exchanging the buffer for 1× PBS using an Illustra NAP-5 column (GE Healthcare).

### Characterization of antibody-coated nPD

Every functionalization step was assessed by electrochemical impedance spectroscopy using a PalmSens4 potentiostat (PalmSens) with a platinum counter electrode and a silver/silver chloride reference electrode. The nPD chips were used as working electrodes in an electrolyte consisting of 5 mM potassium hexacyanoferrate(III) (Sigma-Aldrich) and 5 mM potassium hexacyanoferrate(II) trihydrate (Sigma-Aldrich) in 1× PBS. The nPDs were lastly removed from the chips by ultrasonication, and their functionalization was confirmed by confocal microscopy. nPDs were deposited onto glass-bottom dishes (MatTek) by applying 100 μl of nPD suspension to each overnight. The samples were then incubated with secondary antibodies [Alexa Fluor 594 goat anti-mouse IgG (H+L); 1:1000 dilution; Invitrogen, no. A-11032] for 3 hours, washed three times with 1× PBS, and visualized using an Axio Observer Z1 LSM 800 confocal microscope (Zeiss) equipped with a 40× oil objective. Images were analyzed using Zen software (Zeiss).

### Immunofluorescence and confocal imaging

OSCs were fixed by 4% formaldehyde (prepared from fresh paraformaldehyde; Sigma-Aldrich) in PBS for 1 hour at RT and then washed three times for 15 min in PBS. Free aldehyde groups were quenched with 0.1 M glycine/PBS for 30 min. The samples were blocked and permeabilized in 10% FBS, 5% BSA, and 0.3% Triton X-100 in PBS for 1 hour at RT before incubation with primary antibodies [mouse monoclonal anti-NeuN (1:500; Millipore, no. MAB377), mouse polyclonal anti-GFAP (1:500; Sigma-Aldrich, no. G3898), rabbit polyclonal anti-GABA (1:500; Sigma-Aldrich, no. A2052), mouse

monoclonal anti-GAD67 (1:500 dilution; Sigma-Aldrich, no. MAB5406), guinea pig polyclonal anti-Vglut1 (1:500; Millipore, no. AB5905), rabbit monoclonal anti-ionized calcium-binding adapter molecule 1 (IBA1) (1:400; Invitrogen, no. MA5-36257), rabbit polyclonal anti-GluA2/3 (1:500; Millipore, no. AB1506)] in blocking solution without Triton X-100 for 72 hours at 4°C and under agitation. After washing three times for 15 min with PBS, samples were then incubated under agitation in secondary antibodies [Alexa Fluor 488 goat anti-mouse (1:500 dilution; Invitrogen, no. A-11001), Alexa Fluor 488 goat anti-rabbit (1:500 dilution; Invitrogen, no. A-11008), Alexa Fluor 594 goat anti-mouse (1:500 dilution; Invitrogen, no. A-11032), Alexa Fluor 594 goat anti-rabbit (1:500 dilution; Invitrogen, no. A-11012), and 4′,6-diamidino-2-phenylindole (DAPI; 1:200 dilution; Invitrogen, no. D1306)] for 2 hours RT, washed three times for 15 min in PBS, and mounted onto glass coverslips using Fluoromount-G mounting medium (Invitrogen).

Images were acquired using a Nikon A1R confocal microscope, equipped with 4× (NA 0.20), 20× (NA 0.75), and 40× (NA 0.95) air objectives. Confocal sections were acquired with resolution of 3.1 µm by 3.1 µm (for 4×) and 0.6 µm by 0.6 µm (for 20×) and a step size of 31 µm (4×) and 1.6 µm (20×). Fields of view observed with the 40× objective were acquired via *Z*-stack with a thickness of 12 µm and a 0.62-µm step. Transformation index (TI) was used for assessing microglia's morphofunctional state in saline-treated and nPD-treated OSCs. TI was calculated with the following formula $\mathrm{TI} = \frac{[\text{perimeter of given cell } (\mu m)]^2}{4\pi \times [\text{Area of given cell } (\mu m^2)]}$ and computed by measuring area and perimeter of IBA1 immunopositive cells via Fiji software. Assessment of microglia's proliferation was performed by counting the amount of IBA1 immunoreactive cells per field of view and then computing IBA1-positive cells per square millimeter. Fluorescence intensity of GFAP-associated signal was calculated via Volocity software. The aforementioned experiments aiming at the evaluation of OSC potential neuroinflammatory state after nPD treatment were performed in double and repeated in two different OSCs cultures. ROIs were obtained from the dorsal or ventral part of slice. In focus, slices were smoothed and maximally (for fluorescence and BF images) or minimally (for BF images of nPDs) *Z*-projected using Fiji (*49*).

### Superresolution microscopy

OSCs incubated with nPDs for 24 hours were labeled with a 1:5000 dilution in recording solution of a 1 mM stock solution of LysoTracker Red DND-99 (Invitrogen, L7528) for 30 min at 4°C, washed, and fixed as described above, before an overnight incubation with a 1:100 dilution of concanavalin A (ConA) [stock (1 mg/ml)] under agitation in the cold room. On the next day, samples were stained with DAPI, washed, and mounted. Stacks of structured illumination microscope (SIM) images were taken on a Zeiss Elyra 7 equipped with four lasers [blue (405 nm), green (488 nm), red (561 nm), and far-red (647 nm)] with a 20× objective in Apotome mode. SIM reconstruction was performed with standard settings in Zeiss Zen Black Edition for Elyra. nPDs exhibited slight reflection in all wavelengths, so the signal in far-red was used for identifying nPD positions and subtracted from the other channels before 3D surface reconstruction with Imaris 3.0 software.

### Correlation analysis

The synchronization analysis was based on a bootstrapping method modified by Usmani *et al.* (*11*). Thirty neurons were selected for each field of view, and for each pair of traces, 200,000 – time windows were generated and used to obtain a "real CCF (cross-correlation factor)" distribution with its mean (mreal). The so obtained mreals were divided into three groups, namely, <0.5 (not significant), 0.5 to 0.9, and >0.9 (very significant), and the distribution over these groups compared before and after stimulation using the chi-square test.

### Statistical analysis

Statistical analysis was performed in GraphPad Prism 7.2. The results are presented as box plots with the thick horizontal bars indicating median values, the boxed area as the 25th to 75th percentiles, and whiskers ranging from minimal to maximal values. Single values are given as dots with connecting lines for paired values. Paired Student's *t* test was used for paired values, the Kolmogorov-Smirnoff test was used for the cumulative distributions in Fig. 2F, and the chi-square test was used for cumulative distributions in Fig. 5D.

## SUPPLEMENTARY MATERIALS

Supplementary material for this article is available at https://science.org/doi/10.1126/sciadv.abp9257

View/request a protocol for this paper from *Bio-protocol*.

## REFERENCES AND NOTES


1. J. S. Perlmutter, J. W. Mink, Deep brain stimulation. *Annu. Rev. Neurosci.* **29**, 22–257 (2006).
2. K. Ashkan, P. Rogers, H. Bergman, I. Ughratdar, Insights into the mechanisms of deep brain stimulation. *Nat. Rev. Neurol.* **13**, 548–554 (2017).
3. P. Gupta, N. Balasubramaniam, H.-Y. Chang, F.-G. Tseng, T. S. Santra, A single-neuron: Current trends and future prospects. *Cell* **9**, 1528 (2020).
4. M. C. Romero, M. Davare, M. Armendariz, P. Janssen, Neural effects of transcranial magnetic stimulation at the single-cell level. *Nat. Commun.* **10**, 2642 (2019).
5. M. Diamantaki, S. Coletta, K. Nasr, R. Zeraati, S. Laturnus, P. Berens, P. Preston-Ferrer, A. Burgalossi, Manipulating hippocampal place cell activity by single-cell stimulation in freely moving mice. *Cell Rep.* **23**, 32–38 (2018).
6. B. Knauer, M. C. Stüttgen, Assessing the impact of single-cell stimulation on local networks in rat barrel cortex—A feasibility study. *Int. J. Mol. Sci.* **20**, 2604 (2019).
7. G. Doron, M. Brecht, What single-cell stimulation has told us about neural coding. *Philos. Trans. R. Soc. B Biol. Sci.* **370**, 20140204 (2015).
8. R. Parameswaran, J. L. Carvalho-de-Souza, Y. Jiang, M. J. Burke, J. F. Zimmerman, K. Koehler, A. W. Phillips, J. Yi, E. J. Adams, F. Bezanilla, B. Tian, Photoelectrochemical modulation of neuronal activity with free-standing coaxial silicon nanowires. *Nat. Nanotechnol.* **13**, 260–266 (2018).
9. J. Rivnay, H. Wang, L. Fenno, K. Deisseroth, G. G. Malliaras, Next-generation probes, particles, and proteins for neural interfacing. *Sci. Adv.* **3**, e1601649 (2017).
10. D. Avossa, M. Grandolfo, F. Mazzarol, M. Zatta, L. Ballerini, Early signs of motoneuron vulnerability in a disease model system: Characterization of transverse slice cultures of spinal cord isolated from embryonic ALS mice. *Neuroscience* **138**, 1179–1194 (2006).
11. S. Usmani, E. R. Aurand, M. Medelin, A. Fabbro, D. Scaini, J. Laishram, F. B. Rosselli, A. Ansuini, D. Zoccolan, M. Scarselli, M. De Crescenzi, S. Bosi, M. Prato, L. Ballerini, 3D meshes of carbon nanotubes guide functional reconnection of segregated spinal explants. *Sci. Adv.* **2**, e1600087 (2016).
12. V. Giacco, G. Panattoni, M. Medelin, E. Bonechi, A. Aldinucci, C. Ballerini, L. Ballerini, Cytokine inflammatory threat, but not LPS one, shortens GABAergic synaptic currents in the mouse spinal cord organotypic cultures. *J. Neuroinflammation* **16**, 127 (2019).
13. A. I. Basbaum, D. M. Bautista, G. Scherrer, D. Julius, Cellular and molecular mechanisms of pain. *Cell* **139**, 267–284 (2009).
14. S. C. Koch, D. Acton, M. Goulding, Spinal circuits for touch, pain, and itch. *Annu. Rev. Physiol.* **80**, 189–217 (2018).
15. B. Frias, A. Merighi, Capsaicin, nociception and pain. *Molecules* **21**, 797 (2016).
16. C. Grienberger, A. Konnerth, Imaging calcium in neurons. *Neuron* **73**, 862–885 (2012).
17. M. A. Green, M. J. Keevers, Optical properties of intrinsic silicon at 300 K. *Prog. Photovolt Res. Appl.* **3**, 189–192 (1995).
18. H. Dana, Y. Sun, B. Mohar, B. K. Hulse, A. M. Kerlin, J. P. Hasseman, G. Tsegaye, A. Tsang, A. Wong, R. Patel, J. J. Macklin, Y. Chen, A. Konnerth, V. Jayaraman, L. L. Looger, E. R. Schreiter, K. Svoboda, D. S. Kim, High-performance calcium sensors for imaging activity in neuronal populations and microcompartments. *Nat. Methods* **16**, 649–657 (2019).

19. S. Schoch, G. Cibelli, G. Thiel, Neuron-specific gene expression of synapsin I: Major role of a negative regulatory mechanism. *J. Biol. Chem.* **271**, 3317–3323 (1996).
20. A. J. Todd, Neuronal circuitry for pain processing in the dorsal horn Europe PMC Funders Group. *Nat. Rev. Neurosci.* **11**, 823–836 (2010).
21. R. D'Mello, A. H. Dickenson, Spinal cord mechanisms of pain. *Br. J. Anaesth.* **101**, 8–16 (2008).
22. A. Sagner, J. Briscoe, Establishing neuronal diversity in the spinal cord: A time and a place. *Development* **146**, dev182154 (2019).
23. P. J. Osseward II, S. L. Pfaff, Cell type and circuit modules in the spinal cord. *Curr. Opin. Neurobiol.* **56**, 175–184 (2019).
24. H. L. Chong, P. C. Ruben, Interaction between voltage-gated sodium channels and the neurotoxin, tetrodotoxin. *Channels* **2**, 407–412 (2008).
25. Y. Jiang, R. Parameswaran, X. Li, J. L. Carvalho-de-Souza, X. Gao, L. Meng, F. Bezanilla, G. M. G. Shepherd, B. Tian, Nongenetic optical neuromodulation with silicon-based materials. *Nat. Protoc.* **14**, 1339–1376 (2019).
26. J. F. Herrero, J. M. A. Laird, J. A. Lopez-Garcia, Wind-up of spinal cord neurones and pain sensation: Much ado about something? *Prog. Neurobiol.* **61**, 169–203 (2000).
27. D. Budai, A. A. Larson, The involvement of metabotropic glutamate receptors in sensory transmission in dorsal horn of the rat spinal cord. *Neuroscience* **83**, 571–580 (1998).
28. S. G. Khasabov, S. D. Rogers, J. R. Ghilardi, C. M. Peters, P. W. Mantyh, D. A. Simone, Spinal neurons that possess the substance P receptor are required for the development of central sensitization. *J. Neurosci.* **22**, 9086–9098 (2002).
29. J. Coste, D. L. Voisin, L. S. Miraucourt, R. Dallel, P. Luccarini, Dorsal horn NK1-expressing neurons control windup of downstream trigeminal nociceptive neurons. *Pain* **137**, 340–351 (2008).
30. D. Spicarova, V. Nerandzic, J. Palecek, Update on the role of spinal cord TRPV1 receptors in pain modulation. *Physiol. Res.* **63**, S225–S236 (2014).
31. A. Fabbro, A. Villari, J. Laishram, D. Scaini, F. M. Toma, A. Turco, M. Prato, L. Ballerini, Spinal cord explants use carbon nanotube interfaces to enhance neurite outgrowth and to fortify synaptic inputs. *ACS Nano* **6**, 2041–2055 (2012).
32. H.-Y. Zhou, S.-R. Chen, H. Chen, H.-L. Pan, The glutamatergic nature of TRPV1-expressing neurons in the spinal dorsal horn. *J. Neurochem.* **108**, 305–318 (2009).
33. N. P. Pampaloni, M. Lottner, M. Giugliano, A. Matruglio, F. D'Amico, M. Prato, J. A. Garrido, L. Ballerini, D. Scaini, Single-layer graphene modulates neuronal communication and augments membrane ion currents. *Nat. Nanotechnol.* **13**, 755–764 (2018).
34. C. Torsney, A. B. MacDermott, Disinhibition opens the gate to pathological pain signaling in superficial neurokinin 1 receptor-expressing neurons in rat spinal cord. *J. Neurosci.* **26**, 1833–1843 (2006).
35. W. Zieglgänsberger, Substance P and pain chronicity. *Cell Tissue Res.* **375**, 227–241 (2019).
36. F. Furlan, G. Taccola, M. Grandolfo, L. Guasti, A. Arcangeli, A. Nistri, L. Ballerini, ERG conductance expression modulates the excitability of ventral horn GABAergic interneurons that control rhythmic oscillations in the developing mouse spinal cord. *J. Neurosci.* **27**, 919–928 (2007).
37. J. Dimidschstein, Q. Chen, R. Tremblay, S. L. Rogers, G. A. Saldi, L. Guo, Q. Xu, R. Liu, C. Lu, J. Chu, J. S. Grimley, A. R. Krostag, A. Kaykas, M. C. Avery, M. S. Rashid, M. Baek, A. L. Jacob, G. B. Smith, D. E. Wilson, G. Kosche, I. Kruglikov, T. Rusielewicz, V. C. Kotak, T. M. Mowery, S. A. Anderson, E. M. Callaway, J. S. Dasen, D. Fitzpatrick, V. Fossati, M. A. Long, S. Noggle, J. H. Reynolds, D. H. Sanes, B. Rudy, G. Feng, G. Fishell, A viral strategy for targeting and manipulating interneurons across vertebrate species. *Nat. Neurosci.* **19**, 1743–1749 (2016).
38. D. Avossa, M. D. Rosato-Siri, F. Mazzarol, L. Ballerini, Spinal circuits formation: A study of developmentally regulated markers in organotypic cultures of embryonic mouse spinal cord. *Neuroscience* **122**, 391–405 (2003).
39. O. Kiehn, Decoding the organization of spinal circuits that control locomotion. *Nat. Rev. Neurosci.* **17**, 224–238 (2016).
40. L. Ballerini, M. Galante, M. Grandolfo, A. Nistri, Generation of rhythmic patterns of activity by ventral interneurones in rat organotypic spinal slice culture. *J. Physiol.* **517**, 459–475 (1999).
41. M. Passafaro, V. Piëch, M. Sheng, Subunit-specific temporal and spatial patterns of AMPA receptor exocytosis in hippocampal neurons. *Nat. Neurosci.* **4**, 917–926 (2001).
42. D. E. Clapham, D. Julius, C. Montell, G. Schultz, International union of pharmacology. XLIX. Nomenclature and structure-function relationships of transient receptor potential channels. *Pharmacol. Rev.* **57**, 427–450 (2005).
43. M. J. Caterina, M. A. Schumacher, M. Tominaga, T. A. Rosen, J. D. Levine, D. Julius, The capsaicin receptor: A heat-activated ion channel in the pain pathway. *Nature* **389**, 816–824 (1997).
44. J. Luboeinski, T. Tchumatchenko, Nonlinear response characteristics of neural networks and single neurons undergoing optogenetic excitation. *Netw. Neurosci.* **1**, 852–870 (2020).
45. C. Peirs, R. P. Seal, Neural circuits for pain: Recent advances and current views. *Science* **354**, 578–584 (2016).
46. A. J. Christensen, S. M. Iyer, A. François, S. Vyas, C. Ramakrishnan, S. Vesuna, K. Deisseroth, G. Scherrer, S. L. Delp, In vivo interrogation of spinal mechanosensory circuits. *Cell Rep.* **17**, 1699–1710 (2016).
47. K. Montgomery, S. Iyer, A. Christensen, K. Deisseroth, S. L. Delp, Beyond the brain: Optogenetic control in the spinal cord and peripheral nervous system. *Sci. Transl. Med.* **8**, 337rv5 (2016).
48. C. McClure, K. L. H. Cole, P. Wulff, M. Klugmann, A. J. Murray, Production and titering of recombinant adeno-associated viral vectors. *J. Vis. Exp.* , e3348 (2011).
49. J. Schindelin, I. Arganda-Carreras, E. Frise, V. Kaynig, M. Longair, T. Pietzsch, S. Preibisch, C. Rueden, S. Saalfeld, B. Schmid, J.-Y. Tinevez, D. J. White, V. Hartenstein, K. Eliceiri, P. Tomancak, A. Cardona, Fiji—An open platform for biological image analysis. *Nat. Methods* **9**, 676–682 (2009).
50. M. A. Green, Self-consistent optical parameters of intrinsic silicon at 300K including temperature coefficients. *Sol. Energy Mater. Sol. Cells* **92**, 1305–1310 (2008).


**Acknowledgments:** We thank M. Gigante, G. Cellot, S. Mortal, and M. Lazzarino for help with setting up the laser stimulation setup; the group of P. Heppenstall for help with the AAV production; M. Giugliano for MATLAB code optimization; R. Owen for suggestions in antibody nPD characterization; and S. Usmani for help with initial experiments. This project was funded by HFSP program grant RGP0004/2019 (to L.B., B.T., and L.F.). **Author contributions:** A.T. and M.F. performed all OSC experiments (imaging, immunofluorescence, SIM, and confocal microscopy) and all the related analysis. J.S. and B.T. fabricated and characterized SiNWs. A.T. and D.S. designed the experimental setup and strategy. L.R. performed OSC confocal quantification of resident glial cells and electrophysiology. L.F., A.B.-P., and Y.F. developed the strategy for SiNWs modifications. L.F. and A.E. performed the modified SiNWs synthesis. S.P. characterized the modified SiNWs. B.T., L.F., D.S., and L.B. conceived the study. A.T. and L.B. designed the experimental strategy, interpreted the results, and wrote the manuscript. **Competing interests:** The authors declare that they have no competing interests. **Data and materials availability:** All the data needed to evaluate the conclusions in the paper are present in the paper and/or the Supplementary Materials. Correspondence and requests for materials should be addressed to A.T. (athalham@sissa.it) and L.B. (laura.ballerini@sissa.it).

Submitted 7 March 2022
Accepted 29 June 2022
Published 12 August 2022
10.1126/sciadv.abp9257

ScienceAdvances

# Distributed interfacing by nanoscale photodiodes enables single-neuron light activation and sensory enhancement in 3D spinal explants

Agnes Thalhammer, Mario Fontanini, Jiuyun Shi, Denis Scaini, Luca Recupero, Alexander Evtushenko, Ying Fu, Suraj Pavagada, Andrea Bistrovic-Popov, Ljiljana Fruk, Bozhi Tian, and Laura Ballerini

*Sci. Adv.*, **8** (31), eabp9257.
DOI: 10.1126/sciadv.abp9257







*Science Advances* (ISSN ) is published by the American Association for the Advancement of Science. 1200 New York Avenue NW, Washington, DC 20005. The title *Science Advances* is a registered trademark of AAAS.